IEEE Access
Multidisciplinary ⋮ Rapid Review ⋮ Open Access Journal

Received October 8, 2020, accepted October 27, 2020, date of publication November 3, 2020, date of current version November 18, 2020.

Digital Object Identifier 10.1109/ACCESS.2020.3035585

Optimal Scheduling for Integrated Energy System Considering Scheduling Elasticity of Electric and Thermal Loads

CAN WANG[1,2], (Member, IEEE), SIRUI CHEN[1,2], SHIYI MEI[1,2], RAN CHEN[3], AND HONGLIANG YU[1,2]

[1]Yichang Key Laboratory of Intelligent Operation and Security Defense of Power System, China Three Gorges University, Yichang 443002, China
[2]College of Electrical Engineering and New Energy, China Three Gorges University, Yichang 443002, China
[3]State Grid Hubei Economic Research Institute, Wuhan 430077, China

Corresponding author: Can Wang (xfcancan@163.com)

This work was supported in part by the Scientific Research Project of Hubei Provincial Department of Education under Grant B2019021, and in part by the National Natural Science Foundation of China under Grant 51607105.

ABSTRACT Reasonable scheduling is the basic guarantee for an integrated energy system (IES) to achieve coordinated and efficient operation of multi-energies. For an IES including electric and thermal loads, a demand response (DR) model based on a compensation mechanism is established in this article, and scheduling elasticity (SE) of different types of loads is analyzed to guide users to use energies reasonably and economically. On this basis, an optimization model is established for an IES in accordance with the energy consumption and system operation characteristics. In accordance with the dynamic demands of multi-energies, this model aims at meeting all energy demands with the lowest operation cost. It performs the coordinated optimization for the device output power and the power transmission between multi-energies. To solve the problems of the complex solving process and long computation time, a global optimization algorithm based on a polynomial response surface (PRS) metamodel is proposed in this article. The proposed algorithm adopts a response surface method to fit the optimization model and construct a PRS metamodel to estimate the function values instead of the optimization model, thereby avoiding repeatedly calling the original complex objective function and reducing the computation time. The test results verify the effectiveness of the proposed model and algorithm.

INDEX TERMS Integrated energy system, metamodel, polynomial response surface, scheduling elasticity.

I. INTRODUCTION

Multi-energy mutual aid and energy cascade utilization between different energy systems are effective ways to enhance the comprehensive utilization rate of energies [1]–[4]. As an effective measure to promote energy efficiency, integrated energy systems (IESs) have developed rapidly in recent years [5]. An IES based on the combined heat and power (CHP) unit is one of its important forms [6]. The energy structures and device coupling relationships in the IES are extremely complicated, which greatly increases the difficulty of the system operation and management. Moreover, the intermittency of renewable energy sources greatly affects the safe and reliable operation of IESs [7]–[10]. How to achieve the coordinated and optimal operation of renewable energy sources, energy supply devices, and energy storage devices in the system is a major optimization goal for IES scheduling. It is a significant way to optimize the IES by taking demand response (DR) as a resource to participate in the operation.

Because controllable loads on the demand side have the scheduling elasticity (SE) characteristics, economic measures can be used to guide users to selectively change their energy consumption mode, which can achieve the purpose of energy management [11], [12]. In [13], the thermal dynamic characteristics of district heating networks and buildings were analyzed, and a synchronous response model of the building heat load and a thermal inertia aggregation model were proposed. In [14], the uncertainties of electrical-loads and outdoor temperature were considered, and a day-ahead adaptive robust dispatch model for an IES was proposed. In [15], the physical constraints of power distribution networks, natural gas

The associate editor coordinating the review of this manuscript and approving it for publication was Fabio Massaro.

networks, and district heating networks were considered. The optimal transaction strategy based on the integrated demand response was modeled. However, the above research does not consider the compensation of users. In [16], a coordinated operation scheme with multi-time scales was proposed. This scheme considers the optimal allocation of loads to reduce the operation cost of an industrial multi-energy system. In [17], loads were shifted from the high market price time intervals to the low market price time intervals, which can achieve the goal of maximizing the total profit of a system. In [18], a mathematical model of smart loads in a DR scheme was established to achieve the optimal power generation and load peak scheduling of an IES. However, none of the above studies classifies loads and does not consider that different types of loads have different demand balance relations in different periods, i.e., there exists different SE. To further explore the SE of controllable loads, existing studies have also made a discussion from different perspectives [19]–[21]. The study in [19] proposed a multiparty energy management framework with the electricity and heat DR. Shiftable electric load models and the cuttable thermal load models were analyzed respectively, and an optimization model of users was established. The study in [21] proposed a DR mechanism for an industrial IES. This mechanism can not only reduce interruptible electric loads but also adjust flexible heating and cooling loads. However, the above research is not precise enough to model controllable loads, and only analyze a single type of controllable loads.

In the IESs containing CHP units, the operation of CHP units is nonlinear. Therefore, the optimization problems of the IES based on the DR are mostly multi-constrained nonlinear problems, and the optimization process has the black-box characteristic. The current research has two main solutions to this type of optimization problem. One is to transform the nonlinear problem into a linear programming problem [22], [23], and the other is to solve by an intelligent algorithm [24]–[26]. In [25], an evolutionary optimization algorithm based on the wild goat climbing was proposed, and this algorithm is used to solve the scheduling problem of an IES. In [26], a modified moth swarm algorithm was proposed. The exploration and exploitation abilities of the moth swarm algorithm are improved by employing a learning mechanism. This algorithm is used to minimize the operation cost of a CHP system. The above algorithms are very efficient to solve the black-box problem. However, their optimal solutions require to be generated among a large number of individuals through frequent calculations and complex iterative processes, which is easy to cause slow convergence and local optimal problems.

With the high-order complexity of optimization problems, how to call the high-precision simulation model as little as possible in the optimization process and improve the optimization efficiency becomes particularly important. Metamodels can use sampling points to explore the real process and gradually find the optimal solution to the optimization problem, which is an effective optimization method to solve high time-consuming black-box problems. At present, metamodel types include Kriging models, radial basis function models, polynomial response surface (PRS) models, back-propagation neural network models, and support vector regression models [27]–[29]. The study in [30] proposed a Kriging assisted genetic algorithm for minimizing the generation cost. This algorithm is superior to other heuristic algorithms in the computation time. The study in [31] applied a support vector machine model to the wind power forecasting to discover natural variation structures of wind energy hidden in the historical data. However, the above metamodels have the disadvantage of low fitting accuracy in solving low dimensional optimization problems, which can affect the solution accuracy of the algorithm. In comparison, the PRS metamodel has a higher fitting speed and accuracy [32]. The study in [33] proposed a Bayesian inference approach based on the PRS for the power system dynamic parameter estimation. The study in [34] proposed a probabilistic power flow analysis technique based on the PRS method. This technique can accurately and efficiently estimate the probability distributions and statistics of the power flow response. In [35], the PRS method was applied to a set of parameters to analyze the uncertainties, which can greatly speed up the computation process. The above research results provide a good reference for solving the IES optimization model using the PRS metamodel.

Based on the above analysis, the SE regarding different types of loads is different in the DR. It can further reduce the operation cost of an IES to fully explore the SE characteristics regarding different types of loads. Therefore, an IES optimization model considering the SE regarding different types of loads is proposed in this article. On the one hand, this model can guide users to reduce the load demand during the peak load, and on the other hand, it can make a reasonable allocation of the device output power in the IES to reduce the system operation cost, thereby achieving two-way adjustment between the users and the IES. To solve the problems of complex computation and slow convergence of existing algorithms, this article combines the advantages and characteristics of the metamodel and PRS and proposes a global optimization algorithm based on a PRS metamodel to solve the optimal output of each unit and the total operation cost of an IES.

The main contributions of this article can be summarized as follows:

1) An IES optimization model considering the SE regarding various types of loads is proposed in this article. The proposed model quantifies the SE regarding different types of loads as a DR based on a compensation mechanism and can effectively reduce the operation cost of an IES.
2) A global optimization algorithm based on a PRS metamodel is proposed to solve the proposed optimization model. Different from [30], the proposed algorithm has a higher fitting accuracy and a shorter fitting process. It does not need to repeatedly call the original complex

objective function, which can effectively reduce calculations and time, as well as improve the search efficiency of the globally optimal solution.

3) Based on the time-of-use (TOU) price, the proposed algorithm and optimization model are applied to an IES system considering load SE. This approach effectively optimizes the multi-energy output power and realizes the optimal operation of an IES.

The remainder of the paper is organized as follows. Section II describes the DR model and IES optimization model considering the SE. The global optimization algorithm based on a PRS metamodel is described in Section III. The case study in Section IV illustrates the advantages of the proposed model and algorithm. Section V concludes this article.

II. MATHEMATICAL FORMULATION

A. SE MODEL OF LOAD

Load SE is reflected in its ability to shift or reduce the load demand autonomously at different times. Therefore, this article fully explores the SE regarding various types of loads in different energy systems and divides the loads into shiftable loads and cuttable loads in accordance with the load characteristics. Both types of loads have the advantages of SE, which can realize the flexible changes of demand increase, reduction, or shift within a certain time interval to maintain the balance between supply and demand in an IES. The total demand for the shiftable load remains unchanged before and after the shift, and it is the overall shift. The cuttable load can reduce power or operating time depending on the electricity price. The SE of the thermal load is similar to the electric load, so this section takes the electric load as an example for the model analysis. The optimization variables in the SE model of load are the electricity consumption time L_{shift} of the shiftable load and the cuttable load power $P_{cut,\tau}$. Their power values at each time affect the output power of the power generation and energy storage devices in an IES, thus affecting the operation cost of the IES.

1) SHIFTABLE LOAD

For shiftable load L_{shift}, its power distribution vector L^*_{shift} before participating in the DR is as follows:

$$L^*_{shift} = (0, \cdots, P_{shift,t_S}, P_{shift,t_S+1}, \cdots, P_{shift,t_S+t_D-1}, \cdots, 0) \quad (1)$$

where t_S is the starting time of the electricity consumption, P_{shift,t_S} is the load power before shifting at time t_S, and t_D is the duration time of the electricity consumption.

Suppose the allowable shift interval is $[t_{shift-}, t_{shift+}]$. As the overall shift is required, the starting time and duration time of L_{shift} should be considered, and the 0-1 variable α_τ is used to represent the shift state of L_{shift} at time τ. When $\alpha_\tau = 1$, L_{shift} is shifted from time τ. When $\alpha_\tau = 0$, it means that L_{shift} does not shift. The starting time set S_{shift} of L_{shift} is as follows:

$$\tau \in S_{shift} = [t_{shift-}, t_{shift+} - t_D + 1] \quad (2)$$

If $\tau = t_S$, the shiftable load does not change. If $\tau \neq t_S$, the load is shifted from the original starting time t_S to the new starting time τ. The power distribution vector L_{shift} is as follows:

$$L_{shift} = (0, \cdots, P_{shift,\tau}, P_{shift,\tau+1}, \cdots, P_{shift,\tau+t_D-1}, \cdots, 0) \quad (3)$$

where $P_{shift,\tau}$ is the shifted power at time τ.

The compensation cost F_{shift} of the shiftable load is as follows:

$$F_{shift} = \lambda_1 \sum_{\tau=1}^{T} P_{shift,\tau}\alpha_\tau \quad (4)$$

where λ_1 is the compensation price for load shift per-unit power, and T is the number of time intervals.

2) CUTTABLE LOAD

Cuttable loads can be reduced in part or in whole in accordance with the supply and demand. The 0-1 variable γ_τ is used to represent the reduction state of the cuttable load L_{cut} at time τ. When $\gamma_\tau = 1$, L_{cut} is reduced at time τ. The load power $P_{cut,\tau}$ of L_{cut} participating in the DR at time τ is as follows:

$$P_{cut,\tau} = (1 - \theta\gamma_\tau)P^*_{cut,\tau} \quad (5)$$

where θ is the load reduction coefficient, and the range is $0 < \theta \leq 1$; $P^*_{cut,\tau}$ is the load power of L_{cut} at time τ before scheduling.

The compensation cost F_{cut} of the cuttable load is as follows:

$$F_{cut} = \lambda_2 \sum_{\tau=1}^{T} \gamma_\tau \left(P_{cut,\tau} - P^*_{cut,\tau}\right) \quad (6)$$

where λ_2 is the compensation price for load reduction per-unit power.

Considering the actual requirements of users, the continuous reduction time and the reduction number are constrained to ensure a reasonable load reduction.

$$\begin{cases} T^{\min}_{cut} \leq \sum_{\tau}^{\tau+T^{\min}_{cut}} \gamma_\tau \\ \sum_{\tau}^{\tau+T^{\max}_{cut}} \gamma_\tau \leq T^{\max}_{cut} \end{cases} \quad (7)$$

$$\sum_{\tau}^{T} \gamma_\tau \leq N^{\max} \quad (8)$$

where $T^{\min}_{cut}$ and $T^{\max}_{cut}$ are the minimum and maximum continuous reduction time, respectively; and $N^{\max}$ is the maximum reduction number within the scheduling period.

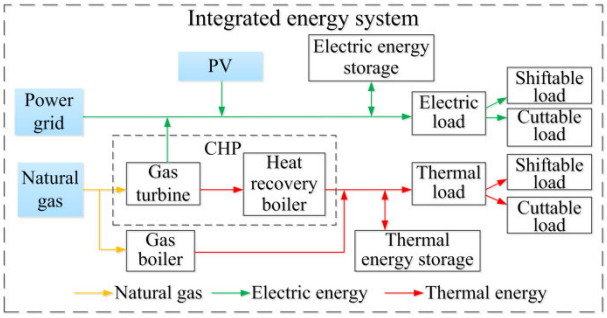

FIGURE 1. Energy flows relationship of the IES.

B. SYSTEM OPTIMIZATION MODEL

A reasonable operation cost is an important prerequisite to popularize the IES. To this end, this article takes the system minimum daily operation cost C_{total} as the objective function. Specifically, the system operation cost includes the fuel cost, start-up and shut-down costs, maintenance cost, power grid purchasing and selling costs, as well as load compensation cost. The fuel cost is generated by CHP units and gas boilers (GBs). The start-up and shut-down costs are generated by the gas turbines (GTs) in CHP units. The maintenance cost is generated by CHP units, GBs, electric energy storage (EES), and thermal energy storage (TES). Fig. 1 shows the IES structure in this article.

$$\min\ C_{total} = C_{fuel} + C_{ss} + C_{om} + C_{grid} + C_{load} \tag{9}$$

where C_{fuel} is the fuel cost, C_{ss} is the start-up and shut-down costs, C_{om} is the maintenance cost, C_{grid} is the power grid purchasing and selling costs, and C_{load} is the total compensation cost of electric and thermal loads.

$$C_{fuel} = \sum_{t=1}^{T}\left(\frac{R_{ng}P_{CHP,t}}{H_{ng}\eta_{CHP}} + \frac{R_{ng}Q_{GB,t}}{H_{ng}\eta_{GB}}\right) \tag{10}$$

$$C_{ss} = \sum_{t=1}^{T}(\max\{0, U_t - U_{t-1}\}\lambda_{SU} + \max\{0, U_{t-1} - U_t\}\lambda_{SD}) \tag{11}$$

$$C_{om} = \sum_{t=1}^{T}\left[k_{CHP}P_{CHP,t} + k_{GB}Q_{GB,t} + k_{EES}\left(P_{EES\_c,t}\eta_{EES\_c} + P_{EES\_d,t}/\eta_{EES\_d}\right) + k_{TES}\left(Q_{TES\_c,t}\eta_{TES\_c} + Q_{TES\_d,t}/\eta_{TES\_d}\right)\right] \tag{12}$$

$$C_{grid} = \sum_{t=1}^{T}R_{price,t}P_{grid,t}\Delta t \tag{13}$$

$$C_{load} = F_{shift} + F_{cut} \tag{14}$$

In (10)-(14), T is the number of time intervals; $R_{ng}$is the natural gas price; H_{ng} is the heating value of natural gas; $P_{CHP,t}$ and $Q_{GB,t}$ are the output electric power of the CHP unit and the output thermal power of the GB at time t, respectively; η_{CHP} and η_{GB} are the electrical efficiency of the CHP unit and the thermal efficiency of the GB, respectively; λ_{SU} and λ_{SD} are the start-up cost coefficient and shut-down cost coefficient, respectively; U_t is the state variable of the CHP unit at time t; a value of 1 denotes that the unit is on, and a value of 0 denotes that the unit is shut down; k_{CHP} and k_{GB} are the maintenance cost coefficients of the CHP unit and GB, respectively; k_{EES} and k_{TES} are the maintenance cost coefficients of the EES and TES, respectively; $P_{EES\_c,t}$ and $P_{EES\_d,t}$ are the charging and discharging power of the EES at time t; η_{EES_c} and η_{EES_d} are the charging and discharging efficiencies of the EES; $Q_{TES\_c,t}$ and $Q_{TES\_d,t}$ are the charging and discharging power of the TES at time t; η_{TES_c} and η_{TES_d} are the charging and discharging efficiencies of the TES; $R_{price,t}$ is the electricity price at time t; and $P_{grid,t}$ is the tie-line power at time t. When $P_{grid,t} > 0$, $R_{price,t}$ adopts the purchasing price; when $P_{grid,t} < 0$, $R_{price,t}$ adopts the selling price.

In the IES optimization model, the optimization variables include the output electric power $P_{CHP,t}$ and the output thermal power $Q_{GB,t}$ in the fuel cost C_{fuel}; the state variable U_t of the CHP unit in the start-up and shut-down costs C_{ss}; the output electric power $P_{CHP,t}$, the output thermal power $Q_{GB,t}$, the charging power $P_{EES\_c,t}$ and the discharging power $P_{EES\_d,t}$ of the EES, the charging power $Q_{TES\_c,t}$ and the discharging power $Q_{TES\_d,t}$ of the TES in the maintenance cost C_{om}; the tie-line power $P_{grid,t}$ in the power grid purchasing and selling costs C_{grid}; and the electricity consumption time L_{shift} of the shiftable electric load, the cuttable electric load power $P_{cut,\tau}$, the electricity consumption time of the shiftable thermal load, and the cuttable thermal load power in the compensation cost C_{load}.

C. CONSTRAINT CONDITIONS

The constraints of the IES optimization model describe the operating range of the system, and the constraint range is from the device characteristics of the CHP unit to the supply and demand balance of the system.

1) OUTPUT POWER CONSTRAINTS

$$P_{CHP,t}^{\min} \le P_{CHP,t} \le P_{CHP,t}^{\max} \tag{15}$$

$$Q_{CHP,t} = \eta_{GT}P_{CHP,t} \tag{16}$$

$$Q_{GB,t}^{\min} \le Q_{GB,t} \le Q_{GB,t}^{\max} \tag{17}$$

where $P_{CHP,t}^{\min}$ and $P_{CHP,t}^{\max}$ are the minimum and maximum output electric power of the CHP unit, $Q_{CHP,t}$ is the output thermal power of the CHP unit at time t, η_{GT} is the electric-heating ratio of the CHP unit, and $Q_{GB,t}^{\min}$ and $Q_{GB,t}^{\max}$ are the minimum and maximum output thermal power of the GB.

2) TIE-LINE POWER CONSTRAINT

$$P_{grid,t}^{\min} \le P_{grid,t} \le P_{grid,t}^{\max} \tag{18}$$

where $P_{grid,t}^{\min}$ and $P_{grid,t}^{\max}$ are the minimum and maximum values of the interactive power between the IES and the power grid, respectively.

3) RAMP UP/DOWN RATE CONSTRAINTS

$$\begin{cases} P_{CHP,t} - P_{CHP,t-1} \le R_{CHP}^{up} \Delta t \\ P_{CHP,t-1} - P_{CHP,t} \le R_{CHP}^{down} \Delta t \end{cases} \tag{19}$$

where R_{CHP}^{up} and R_{CHP}^{down} represent the maximum ramp up and down rates of the CHP unit in adjacent periods, respectively.

4) ENERGY STORAGE CONSTRAINTS

$$0 \le P_{EES\_c,t} \le U_{EES\_c,t} P_{EES\_c,t}^{\max} \tag{20}$$
$$0 \le P_{EES\_d,t} \le U_{EES\_d,t} P_{EES\_d,t}^{\max} \tag{21}$$
$$0 \le Q_{TES\_c,t} \le U_{TES\_c,t} Q_{TES\_c,t}^{\max} \tag{22}$$
$$0 \le Q_{TES\_d,t} \le U_{TES\_d,t} Q_{TES\_d,t}^{\max} \tag{23}$$
$$U_{EES\_c,t} + U_{EES\_d,t} \le 1 \tag{24}$$
$$U_{TES\_c,t} + U_{TES\_d,t} \le 1 \tag{25}$$
$$E_{EES,t}^{\min} \le E_{EES,t} \le E_{EES,t}^{\max} \tag{26}$$
$$E_{TES,t}^{\min} \le E_{TES,t} \le E_{TES,t}^{\max} \tag{27}$$

where $P_{EES\_c,t}^{\max}$ and $P_{EES\_d,t}^{\max}$ are the maximum charging and discharging power of the EES, respectively; $U_{EES\_c,t}$ and $U_{EES\_d,t}$ are the charging and discharging states of the EES, respectively; $Q_{TES\_c,t}^{\max}$ and $Q_{TES\_d,t}^{\max}$ are the maximum charging and discharging power of the TES, respectively; $U_{TES\_c,t}$ and $U_{TES\_d,t}$ are the charging and discharging states of the TES, respectively; $E_{EES,t}^{\min}$ and $E_{EES,t}^{\max}$ are the minimum and maximum capacities of the EES, respectively; $E_{TES,t}^{\min}$ and $E_{TES,t}^{\max}$ are the minimum and maximum capacities of the TES, respectively; and $E_{EES,t}$ and $E_{TES,t}$ are the electric storage capacity of the EES and the thermal storage capacity of the TES at time t. Their calculations are as follows:

$$E_{EES,t} = E_{EES,t-1} + \left[P_{EES\_c,t} \eta_{EES\_c} - \frac{P_{EES\_d,t}}{\eta_{EES\_d}} \right] \Delta t \tag{28}$$

$$E_{TES,t} = E_{TES,t-1} + \left[Q_{TES\_c,t} \eta_{TES\_c} - \frac{Q_{TES\_d,t}}{\eta_{TES\_d}} \right] \Delta t \tag{29}$$

It is assumed that the storage capacity in the last period is the same as the storage capacity in the initial period.

$$E_{EES,0} = E_{EES,T} \tag{30}$$
$$E_{TES,0} = E_{TES,T} \tag{31}$$

where $E_{EES,0}$ and $E_{EES,T}$ are the initial and last storage capacities in the EES, respectively; and $E_{TES,0}$ and $E_{TES,T}$ are the initial and last storage capacities in the TES, respectively.

5) SYSTEM SUPPLY AND DEMAND BALANCE CONSTRAINTS

$$Q_{CHP,t} + Q_{GB,t} + Q_{TES\_d,t} = Q_{load,t} + Q_{TES\_c,t} \tag{32}$$

$$P_{PV,t} + P_{CHP,t} + P_{EES\_d,t} + P_{grid,t} = P_{load,t} + P_{EES\_c,t} \tag{33}$$

where $Q_{load,t}$ is the thermal load power at time t, $P_{PV,t}$ is the photovoltaic (PV) power generation at time t, and $P_{load,t}$ is the electric load power at time t.

III. GLOBAL OPTIMIZATION ALGORITHM BASED ON A PRS METAMODEL

Metamodels are mathematical models that satisfy the required accuracy to replace complex models for numerical calculations or physical experiments with lower calculation cost and higher calculation efficiency. The construction process of metamodels can be divided into two main steps: (1) Based on a sampling design method, the sampling points are constructed; (2) Based on the sampling points, a mathematical model that satisfies the accuracy requirement is obtained by fitting with a mathematical approximate method. Therefore, from the mathematical point of view, metamodels utilize sampling points to construct a function to estimate the response values of unknown points through the fitting or interpolation. In this article, a global optimization algorithm based on a PRS metamodel is proposed by combining the principle of the metamodel with the searching principle of space exploration and region elimination (SERE) technology.

A. LATIN HYPERCUBE SAMPLING

Sample selection is an important prerequisite for constructing a metamodel. It is necessary to select an appropriate sampling method to construct a metamodel with high accuracy and make the number of sampling points within an acceptable range in the process of data sampling. Among random sampling methods, the Latin hypercube sampling (LHS) is a multi-dimensional stratified sampling method. It adopts the stratification principle to randomly sample in the design space, which can not only ensure that the sampling points are not aggregated but also improve the sampling efficiency and has the excellent space coverage [36]. Therefore, this article adopts the LHS to extract sampling points. The LHS includes sampling and sorting. The sampling process of extracting M sampling points from the N-dimensional objective function is as follows:

Step 1: Each dimension of the N-dimensional is divided into M intervals that do not overlap with each other so that each interval has the same probability. A uniform distribution is considered so that each interval is the same length. A total of $M \times N$ intervals are generated.

Step 2: A point is randomly selected with equal probability in each interval of every dimension, denoted as a_{MN}. For N variables, a total of $M \times N$ values are generated, and the resulting matrix is as follows:

$$\psi_{MN} = \begin{bmatrix} a_{11} & a_{12} & \cdots & a_{1N} \\ a_{21} & a_{22} & \cdots & a_{2N} \\ \vdots & \vdots & \vdots & \vdots \\ a_{M1} & a_{M2} & \cdots & a_{MN} \end{bmatrix} \tag{34}$$

Step 3: A point is randomly selected from each column vector of ψ_{MN}, and they are composed into a vector, denoted as $[\omega_{11}, \omega_{12}, \cdots, \omega_{1N}]$.

Step 4: Step 3 should be repeated until M vectors are obtained. Thus, A_{MN} is obtained. Each row vector represents

a set of operational schemes.

$$A_{MN} = \begin{bmatrix} \omega_{11} & \omega_{12} & \cdots & \omega_{1N} \\ \omega_{21} & \omega_{22} & \cdots & \omega_{2N} \\ \vdots & \vdots & \vdots & \vdots \\ \omega_{M1} & \omega_{M2} & \cdots & \omega_{MN} \end{bmatrix} \tag{35}$$

B. CONSTRUCTION OF THE PRS METAMODEL

The PRS method is to construct a PRS metamodel using the data of sampling points to establish the relational expression between the design variables and the objective function, so as to approximate the actual design problem. Because the PRS metamodel has a simple structure, few calculations, and fast solving speed, it can be expressed explicitly. Therefore, this article uses the PRS metamodel to solve the optimization model. The PRS metamodel adopted in this article can be expressed as

$$f(x) = \beta_0 + \sum_{i=1}^{N} \beta_i x_i + \sum_{i=1}^{N} \beta_{ii} x_i^2 + \sum_{i=1}^{N-1} \sum_{j=i+1}^{N} \beta_{ij} x_i x_j \tag{36}$$

where N is the number of input variables; β_0, β_i, β_{ii}, and β_{ij} are polynomial regression coefficients, which together form the polynomial coefficient matrix $\boldsymbol{\beta}$; and x_i is the ith component of N-dimensional independent variables.

The metamodel should meet the interpolation condition that can be expressed as

$$f(x_i) = y_i \quad i = 1, 2, \cdots, M \tag{37}$$

where y_i is the actual objective function value, i.e., the function value in Eq. (9) when the constraints in Eqs. (15)-(33) are satisfied; $f(x_i)$ is the PRS-estimated value, and M is the number of sampling points.

The PRS metamodel is converted into a matrix form that is as follows:

$$\mathbf{F} = \mathbf{X} \cdot \boldsymbol{\beta} \tag{38}$$

where $\mathbf{F}$ is the response value vector of sampling points, and $\mathbf{X}$ is a design matrix of sampling points. In (36):

$$\mathbf{X} = \begin{bmatrix} 1 & x_1^{(1)} & \cdots & x_{N-1}^{(1)} \\ \vdots & \vdots & \ddots & \vdots \\ 1 & x_1^{(M)} & \cdots & x_{N-1}^{(M)} \end{bmatrix} \tag{39}$$

$$\mathbf{F} = [y_1, y_2, \cdots, y_M]^T \tag{40}$$

$$\boldsymbol{\beta} = [\beta_1, \beta_2, \cdots, \beta_N]^T \tag{41}$$

By the least square method, the polynomial coefficient matrix $\boldsymbol{\beta}$ can be solved as

$$\boldsymbol{\beta} = \left(\mathbf{X}^T\mathbf{X}\right)^{-1}\left(\mathbf{X}^T\mathbf{F}\right) \tag{42}$$

The construction process of the PRS metamodel is shown in Fig. 2.

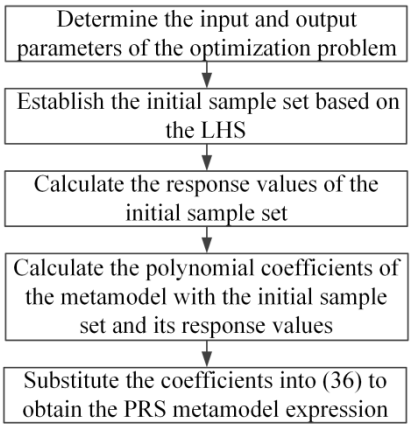

FIGURE 2. Flowchart of the PRS metamodel construction.

To verify the estimation accuracy of the second-order PRS metamodel, a multiple correlation coefficient R^2 [37] is adopted for testing. Its calculation is as follows:

$$R^2 = 1 - \frac{\sum_{i=1}^{M} (y_i - f(x_i))^2}{\sum_{i=1}^{M} (y_i - \bar{y})^2} \tag{43}$$

where $\bar{y}$ is the average value of the actual objective function values. The closer the value of R^2 is to 1, the higher the accuracy of the PRS metamodel estimation.

C. GLOBAL OPTIMIZATION ALGORITHM BASED ON A PRS METAMODEL

For the solution of the optimization problem in an IES, the process of a global optimization algorithm based on a PRS metamodel proposed in this article is shown in Fig.3.

The detailed solution steps of the proposed algorithm are as follows:

Step 1: The parameters, including the rated data of the CHP unit, GB, EES, TES, tie-line, TOU price, and PV output power, are initialized.

Step 2: In accordance with the initialization data, the LHS sampling program is used to generate M sets of initial sampling points based on the constraints in Eqs. (15)-(33), and the sampling points are substituted into Eq. (9) to calculate their actual function values in the proposed IES optimization model.

Step 3: The IES optimization model proposed in this article is fitted to construct a PRS metamodel by Eqs. (36)-(42).

Step 4: The actual objective function values in step 2 are sorted by the SERE technology to find the interval that may contain the optimal solution.

Step 5: The LHS sampling program is used again to generate the new sampling points in Eqs. (9)-(33) for the variables of the IES optimization model in the interval that may contain the optimal solution. The PRS metamodel is used to estimate the objective function values of the new sampling points.

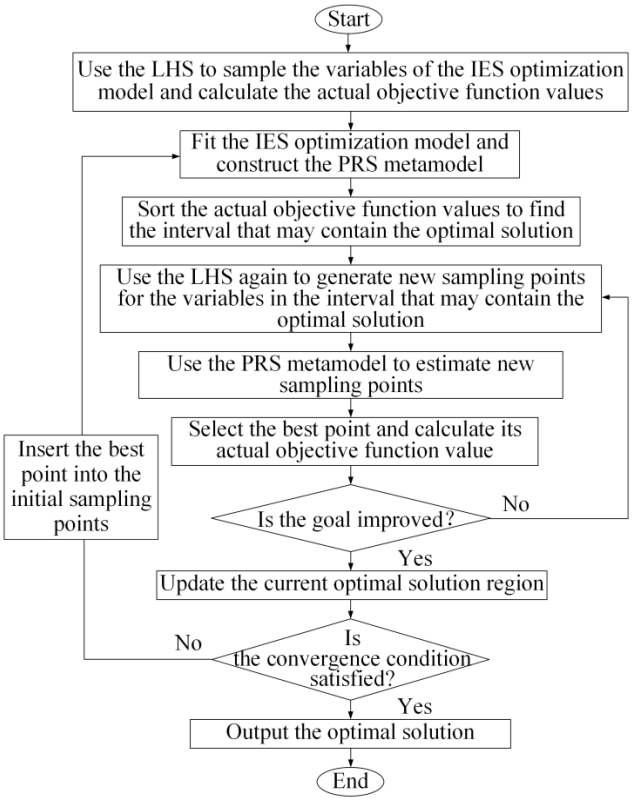

FIGURE 3. Flowchart of the proposed algorithm based on a PRS metamodel.

Step 6: The best values are selected from all estimated function values. The best point is taken into the IES optimization model to calculate its actual objective function value and compare it with the current optimal solution.

Step 7: If the optimal solution is updated, the best point is inserted into the initial sampling points, and the locally optimal solution is updated; otherwise, the current set of the sampling points is not updated, and step 5 is repeated.

Step 8: The next region is examined to determine whether it contains the optimal solution. The globally optimal solution of the current iteration step is obtained by comparing all current local optimal solutions, which is as follows:

$$f_{global} = \min\left(f_{\min 1}, f_{\min 2}, \cdots, f_{\min k}\right) \quad k = 1, \cdots, s \tag{44}$$

Step 9: If the convergence condition is satisfied, the iteration is stopped, and the globally optimal solution is output; otherwise, step 3 is repeated.

The proposed global optimization approach samples the IES at the beginning of each scheduling period and constructs a PRS metamodel by fitting. The calculation of the polynomial coefficient matrix $\boldsymbol{\beta}$ is related to the initial sampling points. When the IES has variations, the initial sampling points of the current scheduling period also have variations, and the calculated polynomial coefficient matrix $\boldsymbol{\beta}$ and the PRS metamodel are also different. Besides, the best point is inserted into the initial sampling points at each iteration, which makes the set of the initial sampling points increase continuously. Therefore, the polynomial coefficient matrix $\boldsymbol{\beta}$ should be calculated based on the initial sampling points at each iteration, thereby obtaining a new PRS metamodel. Based on the above analysis, the polynomial coefficient matrix $\boldsymbol{\beta}$ needs to be recalculated not only in each scheduling period but also at each iteration to obtain an appropriate PRS metamodel. Therefore, in the proposed global optimization approach, the PRS metamodel constructed in this article is dynamically changing and can satisfy the variations of the dynamic IES.

D. GLOBALLY OPTIMAL ANALYSIS OF THE PROPOSED ALGORITHM

Markov chains are a random process with no aftereffect property and are often used to analyze the globally optimal solution. The proposed algorithm is a process of repeated behaviors for sampling, calculating, and estimating. Each behavior is only related to the current solution state and is independent of the previous behavior. Obviously, the solution sequence generated by the proposed algorithm is a Markov chain. Therefore, the Markov chain is used to prove that the proposed algorithm has a globally optimal solution.

Suppose the search space is defined as H. The behaviors for sampling, calculating, and estimating can cause the state transition in the state space, so the transition matrix S, C, and E can be used to represent their influence respectively. The transition matrix of the Markov chain for the proposed algorithm is defined as follows:

$$P = S \times C \times E \tag{45}$$

If the proposed algorithm converges to a globally optimal solution of the problem with probability 1, the proposed algorithm should meet the following two conditions [38]:

(1) For any two pointsx_1 and x_2 in the feasible solution space, x_2 can be obtained by the individual state transition of x_1.

(2) The solution sequence $Q_1, Q_2, \cdots, Q_k$ is monotonic.

For condition (1), if condition (1) is established, the following conditions need to be satisfied [39]:

(a) The solution sequence generated by the proposed algorithm is a finite homogeneous Markov chain.

(b) The Markov chain of the solution sequence generated by the proposed algorithm is ergodic.

Suppose that $Q_k = \{X_1, X_2, \cdots, X_N\}$ is the kth iteration solution of the proposed algorithm, where N is the dimension and X_i is the solution state of the ith iteration. On the one hand, all solutions Q_k are finite, thus forming a finite Markov chain. On the other hand, since the sampling, calculating, estimating, and solution updating of the proposed algorithm are carried out in an independent random process, each solution update has the inheritance with the superior selection. The solution generated in the $k+1$th iteration only depends on the state of the kth iteration and is independent of the transition probability between other states and the number

of iterations. At the same time, a set of solution sequence can be obtained by updating the solution state. Therefore, the solution sequence obtained through a series of independent random transformation processing is a finite homogeneous Markov chain, i.e., condition (a) is satisfied.

To prove condition (b), the following definitions are referenced in this article [40]:

(c) Suppose that P_{ij} is the transition probability matrix of the Markov chain. If $\forall i, j \in H$ and there is $k \geq 1$, which makes $P_{ij}^{k} > 0$, then the Markov chain is irreducible.

(d) If the greatest common divisor of the non-empty set $U = \left\{k | k \geq 1, P_{ij}^{k} > 0, \forall i, j \in H\right\}$ is 1, then the Markov chain is aperiodic.

(e) Suppose that $U_i = \sum_{k}^{\infty} k P_{ij}^{k}$. For the recurrent state i, if $U_i < +\infty$, then i is positive recurrent. In particular, if i is positive recurrent and aperiodic, then the Markov chain is ergodic.

Because the transition probability matrix $P_{ij} = P\{Q_{k+1} = j | Q_k = i, k \geq 1\}$ is only related to the state i and j, where $Q_k > 0$, the transition probability matrix P_{ij} is a positive definite matrix. Therefore, based on definition (c), the solution sequence generated by the proposed algorithm is an irreducible Markov chain. For a given $k > 0$, it can be known from the irreducible Markov chain of the proposed algorithm that $\exists i, j \in H$ makes $P_{ij}^{k} > 0$. It can also be known from definition (d) that $k = 1$. Therefore, there exists a set U whose the greatest common divisor is 1, i.e., the proposed algorithm is an aperiodic irreducible Markov chain. P_{ij} is the transition probability of state i reaching state j through various behaviors. The transition probability of the matrix S, C, and E are all in $(0, 1)$, so $0 < P_{ij} < 1$. Let $\varepsilon = \max\left\{P_{ij} : \forall i, j \in H\right\}$, then it can be known from the Cauchy-Riemann equation and definition (e) that $U_i = \sum_{k}^{\infty} k P_{ij}^{k} \leq \sum_{k}^{\infty} k \varepsilon^{k} < \infty$. Based on the above analysis, it can be concluded that the Markov chain of the proposed algorithm is ergodic, i.e., condition (b) is satisfied.

For condition (2), the behaviors for sampling, calculating, estimating, and solution updating of the proposed algorithm all reflect the optimal solution retention strategy. Moreover, the solution sequence generated by the proposed algorithm is a finite homogeneous Markov chain, and the solution position state of each iteration is updated only when a better solution is obtained. Therefore, the solution of the proposed algorithm in Q_{k+1} is superior to that in Q_k, i.e., the solution sequence $Q_1, Q_2, \cdots, Q_k$ is monotonic non-increasing. Based on the above analysis, it can be concluded that the proposed algorithm satisfies both conditions (1) and (2). Therefore, the proposed algorithm converges to a globally optimal solution to the problem with probability 1.

IV. CASE STUDY

A. BASIC DATA

The topology of the simulation example constructed in this article is shown in Fig. 4, which is mainly composed of the modified IEEE 39-bus power system and the modified Belgium 20-node natural gas system. The test time is 24h, and the time interval is 1h. The natural gas price is 3.24¥/m^3, and the heating value of natural gas is 9.78kWh/m^3. The parameters of 3 CHP units are the same, and the parameters of 3 GBs are the same. The initial capacities of the EES and TES are 20% of the rated capacity. The compensation prices for the shiftable load and the cuttable load are 0.1¥/kWh and 0.2¥/kWh, respectively. The maximum number of reductions of the cuttable load is 8. The TOU price is shown in Table 1. The relevant parameters of each device in the IES are shown in Table 2. The curves of the PV power, electric load power, and thermal load power are shown in Fig. 5.

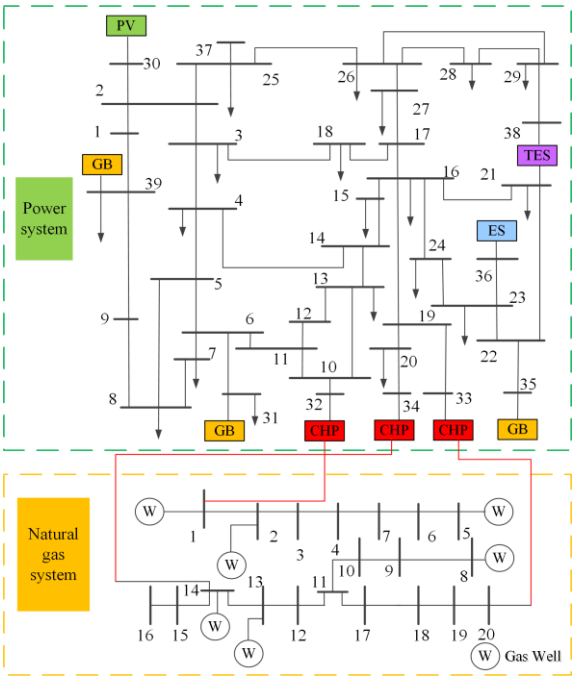

FIGURE 4. The topology of an IES simulation example.

TABLE 1. TOU price.

Period	Time	Purchasing price (¥/kWh)	Selling price (¥/kWh)
Peak	11:00~14:00 18:00~21:00	0.83	0.65
Normal	7:00~10:00 15:00~17:00 22:00~23:00	0.49	0.38
Valley	0:00~6:00	0.17	0.13

To verify the impact of the SE regarding different types of loads in an IES, three cases are compared in this example.

Case 1: The system optimal scheduling does not consider the SE of electric and thermal loads;

Case 2: The system optimal scheduling only considers the SE of shiftable and cuttable electric loads;

Case 3: The system optimal scheduling considers the SE of shiftable and cuttable electric loads and shiftable and cuttable thermal loads.

TABLE 2. Parameter value.

Parameter description	Parameter	Parameter value
CHP	$P^{min}_{CHP,t}$ / $P^{max}_{CHP,t}$ (kW)	0/60
	η_{GT}	0.8
	η_{CHP}	0.386
	R^{up}_{CHP} / R^{down}_{CHP} (kW/h)	80/80
	λ_{SU} / λ_{SD}	0.02/0.03
	k_{CHP}	0.025
GB	η_{GB}	0.83
	$Q^{min}_{GB,t}$ / $Q^{max}_{GB,t}$ (kW)	5/40
	k_{GB}	0.0018
Tie-line	$P^{min}_{grid,t}$ / $P^{max}_{grid,t}$ (kW)	-100/100
EES	$P^{max}_{EES\_c,t}$ / $P^{max}_{EES\_d,t}$ (kW)	40/40
	$E^{min}_{EES,t}$ / $E^{max}_{EES,t}$ (kWh)	36/180
	η_{EES_c} / η_{EES_d}	0.95/0.95
	k_{EES}	0.0018
TES	$Q^{max}_{TES\_c,t}$ / $Q^{max}_{TES\_d,t}$ (kW)	25/25
	$E^{min}_{TES,t}$ / $E^{max}_{TES,t}$ (kWh)	30/150
	η_{TES_c} / η_{TES_d}	0.9/0.9
	k_{TES}	0.0016

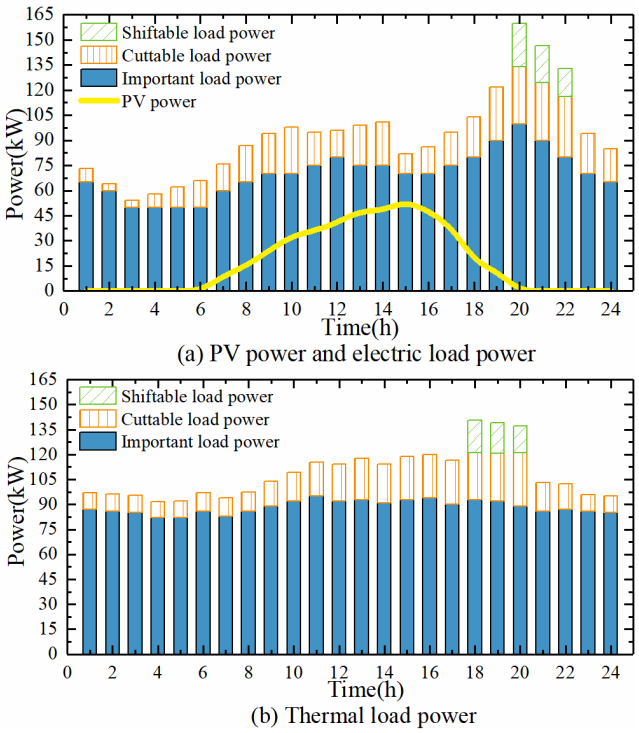

FIGURE 5. The curves of the PV power, electric load power, and thermal load power.

B. ANALYSIS OF OPTIMIZATION RESULTS

The load curve after the optimal scheduling for Case 3 is shown in Fig. 6. Under the condition of satisfying the balance of different energy sources, the optimal scheduling of each device in the IES at each time is shown in Fig. 7.

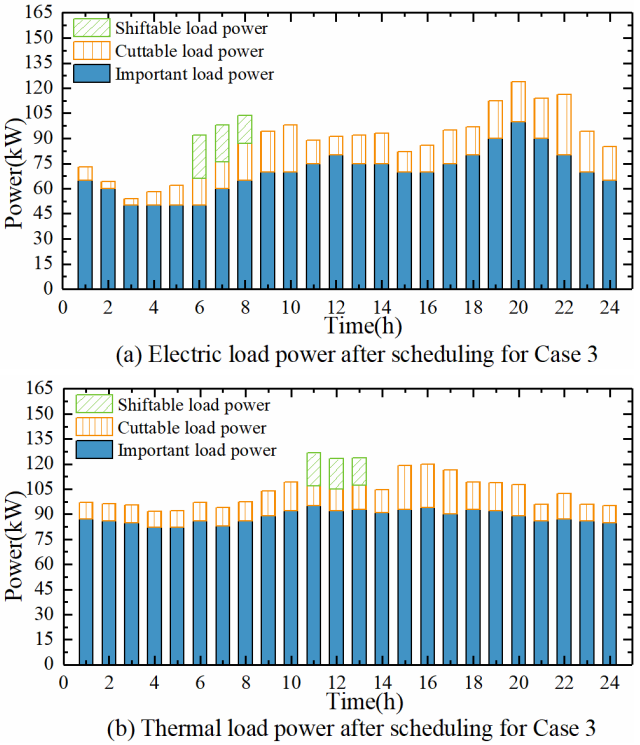

FIGURE 6. Load demand after scheduling for Case 3.

The comparison between Fig. 5(a) and Fig. 6(a) shows that the shiftable electric load shifts from 20:00-22:00 in the original peak load period to 6:00-8:00. This is because the electricity price in this period is relatively low, and the electric balance can be achieved through less electricity purchasing cost, thereby reducing the operation cost. The power consumption in the continuous period remains the same as the original, which ensures the continuity and timing of the shiftable load. Constrained by the number of the reduction time, the cuttable electric load is optimized during the periods of 11:00-14:00 and 18:00-21:00 respectively, which are all in the high electricity price period, thus further reducing the operation cost of the IES. For the thermal load with the SE, it is similar to the electric load. The thermal load can be shifted from the peak load period to the normal period, which plays the role in cutting peaks, and the load can be diminished to further reduce the thermal load.

As can be seen from Fig. 7(a), the electricity purchasing cost of the power grid is less than the operation cost of the CHP units during the period of 1:00-10:00. Therefore, the electric balance is achieved by EES and purchasing electricity. During the high electricity price periods of 11:00-14:00 and 18:00-21:00, the operation cost of the CHP units is less than the electricity purchasing cost, so the CHP units are preferred to provide power for the system. The excess electricity generated is sold to the power grid to increase the system revenue. The EES is charged at the valley electricity price in the whole scheduling period and discharged at the peak electricity price, which makes full use of the

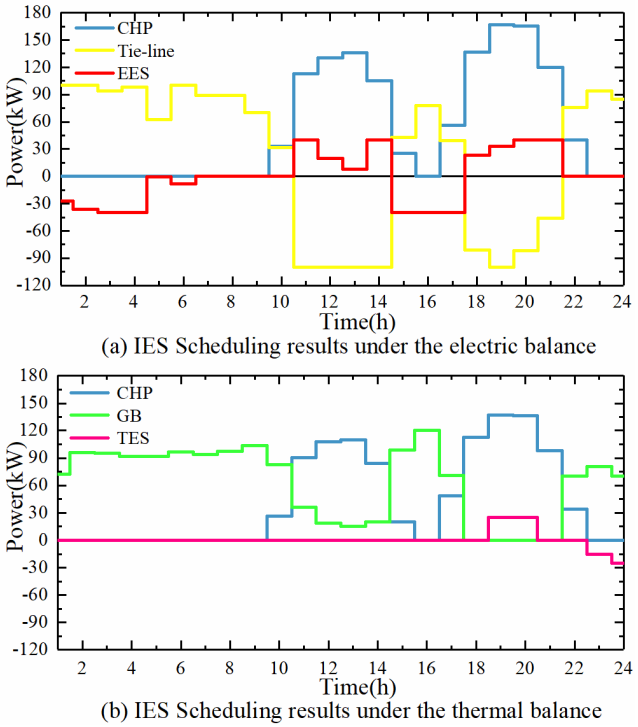

FIGURE 7. Optimal scheduling result for Case 3.

peak-valley electricity price difference to reduce the system operation cost. For the natural gas system, during the period of 1:00-9:00, the CHP units have no heating, and only the GB maintains the thermal balance. During the periods of 10:00-15:00 and 17:00-22:00, the GB only needs to supplement the thermal energy shortage. During the period of 19:00-20:00, the TES stores the excess thermal energy of the CHP units and supplements the thermal energy shortage at 23:00 and 24:00.

To further analyze the impact of the DR on the system operation optimization, the operation results of three Cases are analyzed and compared. As shown in Fig. 8(a), the purchasing energy from the power grid in Case 3 accounts for 24.96% of the total power energy supply, which is greater than that in Case 1. However, the power energy generation of the CHP units in Case 3 accounts for 56.67%, which is less than that in Case 1. In other words, the purchasing power of the entire system increases, and the power generation of the CHP units is reduced. This is because most of the electric load with the SE changes to a period when the electricity price is lower. The electric load with the SE is reduced during the peak electricity price period, thus reducing the power supply. As the thermal load with the SE in Case 3 is reduced in different periods, the heating generation of the GBs is less than that in Case 2.

The cost comparison of the three Cases is shown in Table 3. Further analysis shows that considering the SE regarding different types of loads in different energy systems is effective in improving the IES operation scheduling Although the compensation cost of Case 3 is 45.128 ¥under the load

TABLE 3. Optimization results of different Cases.

Case	Operation cost (¥)	Compensation cost (¥)
1	1746.900	0
2	1724.376	23.203
3	1698.857	45.128

TABLE 4. Solution results of the PRS metamodel for different Orders.

Polynomial order	Computation time (s)	R^2
First-order	52	0.954
Second-order	54	0.981
Third-order	59	0.983

compensation price set in this article, its operation cost is reduced by 2.75% and 1.48% compared to those of Cases 1 and 2, respectively. Therefore, considering the SE regarding different types of loads in different energy systems not only plays a role in cutting peaks and filling valleys but also reduces the operation cost of the IES.

The polynomial order of a PRS metamodel directly affects the accuracy of the estimated value. To analyze the influence of polynomial order on the proposed algorithm, this article uses the first-order, second-order, and third-order PRS metamodels to fit and solve the IES optimization model. The solution results of the PRS metamodel for different orders are shown in Table 4. The first-order PRS metamodel has the shortest computation time, but its value of R^2 is 2.75% and 2.95% lower than the values of R^2 regarding the second-order and third-order PRS metamodels, respectively. This can reduce the estimation accuracy. The third-order PRS metamodel has the longest computation time. This is because the number of coefficients in the PRS metamodel and the computational burden increase with the increase of the order, which results in the increase of the sampling time and the computation time of polynomial coefficients. Moreover, the value of R^2 regarding the third-order PRS metamodel is only 0.20% higher than that of the second-order PRS metamodel, but the computation time of the third-order PRS metamodel is 5s longer than that of the second-order PRS metamodel. It is obvious that the cost of the computation time regarding the third-order PRS metamodel is too high to improve the accuracy of 0.20%.

Based on the above analysis, the second-order PRS metamodel not only has a higher solution accuracy but also has a faster solution speed. Therefore, the second-order PRS metamodel used in this article is good enough to fit an IES optimization model.

C. COMPARATIVE ANALYSIS OF DIFFERENT ALGORITHMS

1) COMPARATIVE ANALYSIS WITH INTELLIGENT SOLUTION ALGORITHMS

In this article, the genetic algorithm (GA), the Kriging algorithm, and the proposed algorithm are used to calculate the optimal solution of Case 3. The convergence curves of the three algorithms are shown in Fig. 9. The calculated operation cost in Fig. 9 is the average value of each algorithm after running 10 times. As shown in Fig. 9, all three algorithms approach an optimal solution stably in the middle and late

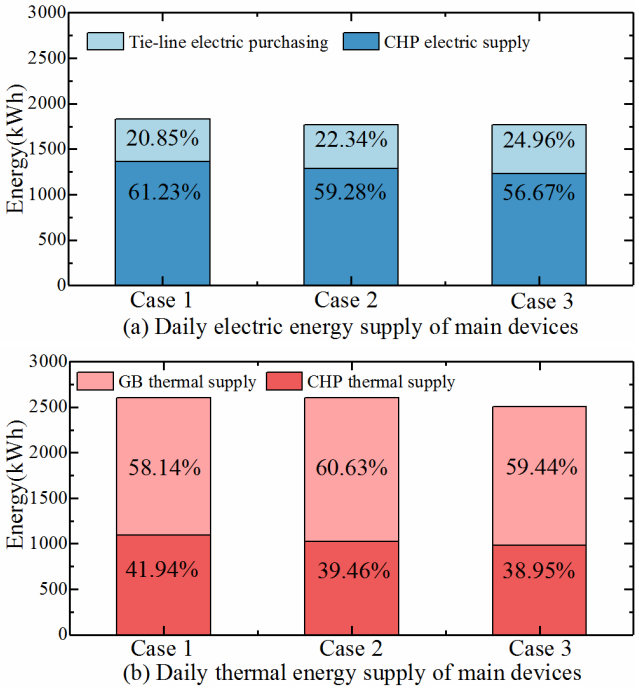

FIGURE 8. Daily energy supply in Cases 1-3.

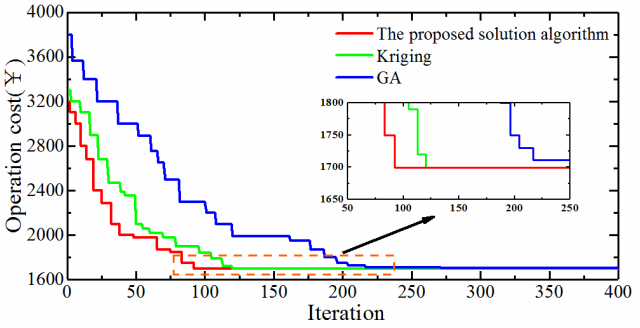

FIGURE 9. Iterative solving process of three algorithms.

TABLE 5. Comparative analysis of algorithm performance.

Algorithm	Computation time (s)	Number of iterations	Optimal solution (¥)
GA	115	272	1703.384
Kriging	61	116	1699.013
PRS	54	92	1698.857

TABLE 6. Comparative analysis of solver performance.

Algorithm	Computation time (s)	Optimal solution (¥)
IPOPT	69	1702.305
BARON	87	1700.969
PRS	54	1698.857

stages, and there is no obvious better solution for a long time. Therefore, it can be concluded that the optimal solution of the algorithm proposed in this article is very close to the actual globally optimal solution. It can be seen that the GA falls into local optimum after 120 iterations, while the Kriging and the proposed algorithm effectively enhance the global search ability by the metamodel principle. In comparison, the proposed algorithm first reaches a stable convergence value, which reflects the advantage of the proposed algorithm in the convergence speed.

To verify the calculation efficiency of the algorithm proposed in this article, the computation time of the three algorithms is counted in this article, and the calculation results are shown in Table 5. In terms of the computation time, the proposed algorithm reduces the search time of the optimal solution compared with the GA and Kriging because the proposed algorithm adopts the SERE technology to reduce the search space. The computation time of the proposed algorithm is reduced by 11.48% compared with that of the Kriging that also adopts the metamodel principle. The proposed algorithm converges to the optimal solution when the number of iterations reaches 92 and achieves stability faster than the GA and Kriging. This shows that the proposed algorithm has better convergence. In terms of the optimization results, the optimal solution of the proposed algorithm is lower than that of the GA and Kriging. It can be seen that the proposed algorithm can improve the solution accuracy while maintaining the overall speed.

2) COMPARATIVE ANALYSIS WITH NONLINEAR SOLVERS

To further verify the effectiveness of the proposed algorithm, the IPOPT solver, the BARON solver, and the proposed algorithm are used to solve the proposed optimization model. The average optimization results of the three algorithms after running independently for 10 times are shown in Table 6. As far as the calculation efficiency is concerned, the proposed algorithm uses the SERE technology to reduce the computation time by 37.93% compared with the BARON solver. Therefore, the proposed algorithm can find the optimal solution faster than the BARON solver. The proposed algorithm simplifies the original complex function through a metamodel, thus reducing the computation time by 21.74% compared with the IPOPT solver. In terms of the optimal solution, the optimal solution of the proposed algorithm is also better than that of the other two solvers.

The proposed algorithm effectively simplifies the complexity of the objective function and takes into account both the global search and local search capabilities through the PRS metamodel fitting and the application of the SERE technology. Therefore, the proposed algorithm is superior to other algorithms in terms of the solution accuracy and convergence speed in solving the complex nonlinear IES scheduling problem.

V. CONCLUSION

Aiming at the complex optimization scheduling problem of the IES with the CHP units, this article proposes to consider the SE regarding different types of loads for the scheduling, constructs an IES optimization model considering the load SE, and designs a global optimization algorithm based on a PRS metamodel. The significant advantages of the model and algorithm proposed in this article are as follows:

(1) Considering the SE regarding different types of loads of different energy systems in the IES with the CHP units, the operation cost of the IES is greatly reduced by the compensation mechanism.

(2) By combining the PRS metamodel with the SERE technology, the proposed algorithm simplifies the complexity of the objective function and reduces the number of calls to the original complex objective function, thus improving the convergence speed and the solution accuracy.

By analyzing the characteristics of different types of loads, this article studies their SE in the IES. In the future, the SE of the transferrable load will be analyzed and modeled. Considering the complex power interaction problem in the combined cooling, heating, and power regional IES, how to apply metamodel technology to this optimization problem is the next step of the research.

REFERENCES

[1] C. Wang, T. Tian, Z. Xu, S. Cheng, S. Liu, and R. Chen, "Optimal management for grid-connected three/single-phase hybrid multimicrogrids," *IEEE Trans. Sustain. Energy*, vol. 11, no. 3, pp. 1870–1882, Jul. 2020.

[2] L. Xi, Z. Zhang, B. Yang, L. Huang, and T. Yu, "Wolf pack hunting strategy for automatic generation control of an islanding smart distribution network," *Energy Convers. Manage.*, vol. 122, pp. 10–24, Aug. 2016.

[3] C. Wang, X. Li, T. Tian, Z. Xu, and R. Chen, "Coordinated control of passive transition from grid-connected to islanded operation for three/single-phase hybrid multimicrogrids considering speed and smoothness," *IEEE Trans. Ind. Electron.*, vol. 67, no. 3, pp. 1921–1931, Mar. 2020.

[4] B. Zhu, F. Ding, and D. M. Vilathgamuwa, "Coat circuits for DC–DC converters to improve voltage conversion ratio," *IEEE Trans. Power Electron.*, vol. 35, no. 4, pp. 3679–3687, Apr. 2020.

[5] Z. Huang, B. Fang, and J. Deng, "Multi-objective optimization strategy for distribution network considering V2G-enabled electric vehicles in building integrated energy system," *Protection Control Mod. Power Syst.*, vol. 5, no. 1, pp. 48–55, Jan. 2020.

[6] Y. Zhou, W. Hu, Y. Min, and Y. Dai, "Integrated power and heat dispatch considering available reserve of combined heat and power units," *IEEE Trans. Sustain. Energy*, vol. 10, no. 3, pp. 1300–1310, Jul. 2019.

[7] S. Liu, L. Liu, Y. Fan, L. Zhang, Y. Huang, T. Zhang, J. Cheng, L. Wang, M. Zhang, R. Shi, and D. Mao, "An integrated scheme for online dynamic security assessment based on partial mutual information and iterated random forest," *IEEE Trans. Smart Grid*, vol. 11, no. 4, pp. 3606–3619, Jul. 2020, doi: 10.1109/TSG.2020.2991335.

[8] Y. Liu, N. Yang, B. Dong, L. Wu, J. Yan, X. Shen, C. Xing, S. Liu, and Y. Huang, "Multi-lateral participants decision-making: A distribution system planning approach with incomplete information game," *IEEE Access*, vol. 8, pp. 88934–88950, 2020.

[9] B. Zhu, Q. Zeng, Y. Chen, Y. Zhao, and S. Liu, "A dual-input high step-up DC/DC converter with ZVT auxiliary circuit," *IEEE Trans. Energy Convers.*, vol. 34, no. 1, pp. 161–169, Mar. 2019.

[10] N. Yang, Y. Huang, D. Hou, S. Liu, D. Ye, B. Dong, and Y. Fan, "Adaptive nonparametric kernel density estimation approach for joint probability density function modeling of multiple wind farms," *Energies*, vol. 12, no. 7, pp. 1356–1370, Apr. 2019.

[11] C. Zhang, Y. Xu, Z. Y. Dong, and K. P. Wong, "Robust coordination of distributed generation and price-based demand response in microgrids," *IEEE Trans. Smart Grid*, vol. 9, no. 5, pp. 4236–4247, Sep. 2018.

[12] A. Silani and M. J. Yazdanpanah, "Distributed optimal microgrid energy management with considering stochastic load," *IEEE Trans. Sustain. Energy*, vol. 10, no. 2, pp. 729–737, Apr. 2019.

[13] S. Lu, W. Gu, K. Meng, S. Yao, B. Liu, and Z. Y. Dong, "Thermal inertial aggregation model for integrated energy systems," *IEEE Trans. Power Syst.*, vol. 35, no. 3, pp. 2374–2387, May 2020.

[14] S. Lu, W. Gu, S. Zhou, S. Yao, and G. Pan, "Adaptive robust dispatch of integrated energy system considering uncertainties of electricity and outdoor temperature," *IEEE Trans. Ind. Informat.*, vol. 16, no. 7, pp. 4691–4702, Jul. 2020.

[15] P. Liu, T. Ding, Z. Zou, and Y. Yang, "Integrated demand response for a load serving entity in multi-energy market considering network constraints," *Appl. Energy*, vol. 250, pp. 512–529, Sep. 2019.

[16] C. Zhang, Y. Xu, Z. Dong, and L. Yang, "Multitimescale coordinated adaptive robust operation for industrial multienergy microgrids with load allocation," *IEEE Access*, vol. 16, no. 5, pp. 3061–3063, 2020.

[17] M. Alipour, B. Mohammadi-Ivatloo, and K. Zare, "Stochastic scheduling of renewable and CHP-based microgrids," *IEEE Trans. Ind. Informat.*, vol. 11, no. 5, pp. 1049–1058, Oct. 2015.

[18] B. V. Solanki, A. Raghurajan, K. Bhattacharya, and C. A. Cañizares, "Including smart loads for optimal demand response in integrated energy management systems for isolated microgrids," *IEEE Trans. Smart Grid*, vol. 8, no. 4, pp. 1739–1748, Jul. 2017.

[19] N. Liu, L. He, X. Yu, and L. Ma, "Multiparty energy management for grid-connected microgrids with heat- and electricity-coupled demand response," *IEEE Trans. Ind. Informat.*, vol. 14, no. 5, pp. 1081–1089, May 2018.

[20] C. Wang, S. Mei, X. Li, S. Kang, and H. Wang, "Seamless transition control strategy for three/single-phase multimicrogrids during unintentional islanding scenarios," *Int. J. Electr. Power Energy Syst.*, 2021, doi: 10.1016/j.ijepes.2020.106730.

[21] Z. Jiang, Q. Ai, and R. Hao, "Integrated demand response mechanism for industrial energy system based on multi-energy interaction," *IEEE Access*, vol. 7, pp. 66336–66346, 2019.

[22] L. Wang, G. Wang, Q. Li, and M. Sun, "Robust optimisation scheduling of CCHP systems with multi-energy based on minimax regret criterion," *IET Gener., Transmiss. Distrib.*, vol. 10, no. 9, pp. 2194–2201, Jun. 2016.

[23] Z. Yang, K. Xie, J. Yu, H. Zhong, N. Zhang, and Q. Xia, "Stochastic optimal operation of microgrid based on chaotic binary particle swarm optimization," *IEEE Trans. Power Syst.*, vol. 34, no. 2, pp. 1315–1324, Mar. 2019.

[24] L. Xi, J. Chen, Y. Huang, Y. Xu, L. Liu, Y. Zhou, and Y. Li, "Smart generation control based on multi-agent reinforcement learning with the idea of the time tunnel," *Energy*, vol. 153, pp. 977–987, Jun. 2018.

[25] A. Shefaei and B. Mohammadi-Ivatloo, "Wild goats algorithm: An evolutionary algorithm to solve the real-world optimization problems," *IEEE Trans. Ind. Informat.*, vol. 14, no. 7, pp. 2951–2961, Jul. 2018.

[26] E. E. Elattar, "Optimal power flow of a power system incorporating stochastic wind power based on modified moth swarm algorithm," *IEEE Access*, vol. 7, pp. 89581–89593, 2019.

[27] S. Deng, R. El Bechari, S. Brisset, and S. Clénet, "Iterative Kriging-based methods for expensive black-box models," *IEEE Trans. Magn.*, vol. 54, no. 3, pp. 1–4, Mar. 2018.

[28] X. Dong, J. Dong, G. Sun, Y. Duan, L. Qi, and H. Yu, "Learning-based texture synthesis and automatic inpainting using support vector machines," *IEEE Trans. Ind. Electron.*, vol. 66, no. 6, pp. 4777–4787, Jun. 2019.

[29] F. Liu, W. Huo, Y. Han, S. Yang, and X. Li, "Study on network security based on PCA and BP neural network under green communication," *IEEE Access*, vol. 8, pp. 53733–53749, 2020.

[30] Z. Deng, M. D. Rotaru, and J. K. Sykulski, "Kriging assisted surrogate evolutionary computation to solve optimal power flow problems," *IEEE Trans. Power Syst.*, vol. 35, no. 2, pp. 831–839, Mar. 2020.

[31] Q. Hu, S. Zhang, M. Yu, and Z. Xie, "Short-term wind speed or power forecasting with heteroscedastic support vector regression," *IEEE Trans. Sustain. Energy*, vol. 7, no. 1, pp. 241–249, Jan. 2016.

[32] D. Zhao and D. Xue, "A comparative study of metamodeling methods considering sample quality merits," *Struct. Multidisciplinary Optim.*, vol. 42, no. 6, pp. 923–938, Dec. 2010.

[33] Y. Xu, C. Huang, X. Chen, L. Mili, C. H. Tong, M. Korkali, and L. Min, "Response-surface-based Bayesian inference for power system dynamic parameter estimation," *IEEE Trans. Smart Grid*, vol. 10, no. 6, pp. 5899–5909, Nov. 2019.

[34] Z. Ren, W. Li, R. Billinton, and W. Yan, "Probabilistic power flow analysis based on the stochastic response surface method," *IEEE Trans. Power Syst.*, vol. 31, no. 3, pp. 2307–2315, May 2016.

[35] D. Han, J. Ma, and R.-M. He, "Multi-parameter uncertainty analysis in power system dynamic simulation: A new solution based on the stochastic response surface method and trajectory sensitivity method," *Electr. Power Compon. Syst.*, vol. 40, no. 5, pp. 480–496, Mar. 2012.

[36] Q. Xu, Y. Yang, Y. Liu, and X. Wang, "An improved Latin hypercube sampling method to enhance numerical stability considering the correlation of input variables," *IEEE Access*, vol. 5, pp. 15197–15205, 2017.

[37] Y. Li, M. Li, Z. Liu, and C. Li, "Combining Kriging interpolation to improve the accuracy of forest aboveground biomass estimation using remote sensing data," *IEEE Access*, vol. 8, pp. 128124–128139, 2020.
[38] T. Back, *Evolutionary Algorithms in Theory and Practice*. New York, NY, USA: Oxford Univ. Press, 1996, pp. 21–28.
[39] J. Liu, W. Zhong, and L. Jiao, "A multiagent evolutionary algorithm for constraint satisfaction problems," *IEEE Trans. Syst. Man, Cybern. B, Cybern.*, vol. 36, no. 1, pp. 54–73, Feb. 2006.
[40] D. Wu, S. Xu, and F. Kong, "Convergence analysis and improvement of the chicken swarm optimization algorithm," *IEEE Access*, vol. 4, pp. 9400–9412, 2016.

CAN WANG (Member, IEEE) was born in Hubei, China. He received the Ph.D. degree in electrical engineering from the South China University of Technology, Guangzhou, China, in 2017.

He is currently a Lecturer in Electrical Engineering with the College of Electrical Engineering and New Energy, China Three Gorges University, Yichang, China. His current research interests include distributed generation, microgrid operation and control, and smart grids.

Dr. Wang serves as the Co-Chair of the Special Session on Power Systems with Penetration of RE and EV at IEEE IGBSG 2019. He is also an Active Reviewer of the IEEE TRANSACTIONS ON SUSTAINABLE ENERGY, IEEE TRANSACTIONS ON INDUSTRIAL ELECTRONICS, IEEE SYSTEMS JOURNAL, *IET Power Electronics*, *IET Renewable Power Generation*, and IEEE ACCESS.

SIRUI CHEN was born in Hubei, China. She is currently pursuing the M.S. degree in electrical engineering with China Three Gorges University, Yichang, China. Her research interests include distributed generation and microgrid energy management.

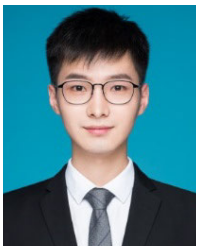

SHIYI MEI was born in Anhui, China. He is currently pursuing the M.S. degree in electrical engineering with China Three Gorges University, Yichang, China. His research interests include distributed generation and microgrid operation and control.

RAN CHEN received the M.S. degree in electrical engineering from the Wuhan University of Technology, Wuhan, China, in 2013. He is currently with the State Grid Hubei Economic Research Institute. His current research interests include microgrid operation and coordinated control.

HONGLIANG YU was born in Hubei, China. He is currently pursuing the M.S. degree in electrical engineering with China Three Gorges University, Yichang, China. His research interests include distributed generation and microgrid operation and control.